J|A|C|S
ARTICLES
Published on Web 04/12/2007

Tunneling in Green Tea: Understanding the Antioxidant Activity of Catechol-Containing Compounds. A Variational Transition-State Theory Study

Ismael Tejero,[†] Núria González-García,[†] Àngels González-Lafont,*[,†,‡] and José M. Lluch[†,‡]

Departament de Química and Institut de Biotecnologia i de Biomedicina, Universitat Autònoma de Barcelona, 08193 Bellaterra (Barcelona), Spain

Received May 30, 2006; E-mail: angels@klingon.uab.es

Abstract: The catechol functionality present in the catechins is responsible for the protective effects exerted by green tea against a wide range of human diseases. High-level electronic structure calculations and canonical variational transition-state theory including multidimensional tunneling corrections have allowed us to understand the key factors of the antioxidant effectiveness of the catechol group. This catechol group forms two hydrogen bonds with the two oxygen atoms of the lipid peroxyl radical, leading to a very compact reactant complex. This fact produces an extremely narrow adiabatic potential-energy profile corresponding to the hydrogen abstraction by the peroxyl radical, which makes it possible for a huge tunneling contribution to take place. So, quantum-mechanical tunneling highly increases the corresponding rate constant value, in such a way that catechins become able to trap the lipid peroxyl radicals in a dominant competition with the very damaging free-radical chain-lipid peroxidation reaction.

1. Introduction

Free-radical-mediated peroxidation of membrane lipids and oxidative damage of DNA are associated with a variety of chronic health problems, such as cancer, inflammation, atherosclerosis, neurodegenerative processes like Alzheimer's and Parkinson's diseases, and aging.[1−3] The radical formation is usually caused by light, heat, metal, or irradiation. Once a first free radical R· (often an alkyl radical) has been generated, it reacts with oxygen to produce a peroxyl radical ROO· which in the presence of a lipid LH initiates a free-radical chain-lipid peroxidation:

$$\mathrm{ROO}\cdot + \mathrm{LH} \rightarrow \mathrm{ROOH} + \mathrm{L}\cdot \quad (1)$$

$$\mathrm{L}\cdot + \mathrm{O_2} \rightarrow \mathrm{LOO}\cdot \quad (2)$$

$$\mathrm{LOO}\cdot + \mathrm{LH} \rightarrow \mathrm{LOOH} + \mathrm{L}\cdot \quad (3)$$

The lipid (L·) and lipid peroxyl (LOO·) radicals act as chain propagators converting lipid molecules into lipid hydroperoxyde LOOH. Reaction 2 is very fast, ca. 10^9 M^{-1} s^{-1}, whereas the hydrogen-transfer reaction (3) is much slower, typically 10^1 M^{-1} s^{-1}.[4]

Vitamin E is the most important lipophilic antioxidant in living organisms.[5−7] α-Tocopherol (TocH), the most abundant and active form of vitamin E, is the major endogenous lipid-soluble chain-breaking antioxidant in human plasma and low-density lipoprotein (LDL).[8−11] α-TocH can break the free-radical chain reaction, trapping the LOO· radicals by a hydrogen abstraction reaction:

$$\mathrm{LOO}\cdot + \alpha\text{-TocH} \rightarrow \mathrm{LOOH} + \alpha\text{-Toc}\cdot \quad (4)$$

thus producing LOOH and α-tocopheroxyl radical (α-Toc·). The problem at this point is that α-TocH might become a prooxidant[12] via an α-TocH-mediated peroxidation:

$$\alpha\text{-Toc}\cdot + \mathrm{LH\ (or\ LOOH)} \rightarrow \alpha\text{-TocH} + \mathrm{L}\cdot\ (\mathrm{or\ LOO}\cdot) \quad (5)$$

To suppress the prooxidant action, α-TocH is regenerated by the reactions of α-Toc· with the endogenous antioxidants ubiquinol and vitamin C.[13,14]

On the other hand, flavonoids are the most common and active edible antioxidants. These naturally ocurring polyphenolic

[†] Departament de Química.
[‡] Institut de Biotecnologia i de Biomedicina.

(1) Commenges, D.; Scotet, V.; Renaud, S.; Jacqmin-Gadda, H.; Barberger-Gateau, P.; Dartigues, J. F. *Eur. J. Epidemiol.* **2000**, *16*, 357−363.
(2) Whitehead, T. P.; Robinson, D.; Allaway, S.; Syms, J.; Hale, A. *Clin. Chem.* **1995**, *41*, 32−35.
(3) Hertog, M. G. L.; Feskens, E. J. M.; Hollman, P. C. H.; Katan, M. B.; Kromhout, D. *Lancet* **1993**, *342*, 1007−1011.
(4) Porter, N. A. *Acc. Chem. Res.* **1986**, *19*, 262−268.
(5) Hacquebard, M.; Carpentier, Y. A. *Curr. Opin. Clin. Nutr.* **2005**, *8*, 133−138.
(6) Valk, E. E. J.; Hornstra, G. *Int. J. Vitam. Nutr. Res.* **2000**, *70*, 31−42.
(7) Pryor, W. A. *Free Radical Biol. Med.* **2000**, *28*, 141−164.
(8) Jiang, X. C.; Tall, A. R.; Qin, S.; Lin,M.; Schneider,M.; Lalanne, F.; Deckert, V.; Desrumaux, C.; Athias, A.; Witztum, J. L.; Lagrost, L. *J. Biol. Chem.* **2002**, *277*, 31850−31856.
(9) Burton, G. W.; Traber, M. G.; Acuff, R. V.; Walters, D. N.; Kayden, H.; Hughes, L.; Ingold, K. U. *Am. J. Clin. Nutr.* **1998**, *67*, 669−684.
(10) Thomas, S. R.; Davies, M. J.; Stocker, R. *Chem. Res. Toxicol.* **1998**, *11*, 484−494.
(11) Thomas, S. R.; Witting, P. K.; Stocker, R. *J. Biol. Chem.* **1996**, *271*, 32714−32721.
(12) Niki, E.; Noguchi, N. *Acc. Chem. Res.* **2004**, *37*, 45−51.
(13) Bowry, V. W.; Stocker, R. *J. Am. Chem. Soc.* **1993**, *115*, 6029−6044.
(14) Mukai, K.; Itoh, S.; Morimoto, H. *J. Biol. Chem.* **1992**, *267*, 22277−22281.

10.1021/ja063766t CCC: $37.00

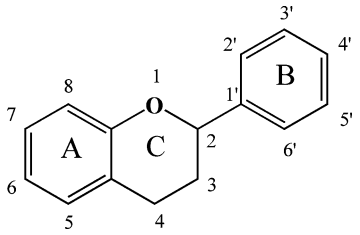

Figure 1. Basic flavonoid structure.

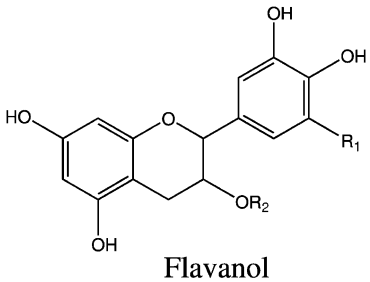

Flavanol

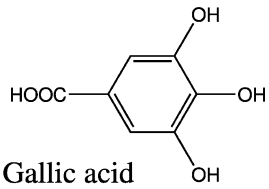

Gallic acid

Flavanols	R1	R2
Epicatechin	H	H
EGC	OH	H
ECG	H	Gallate
EGCG	OH	Gallate

Figure 2. The four different catechins (flavanols) as the main components of green tea.

pigment compounds are present in substantial amounts in plants, fruits, and vegetables.[15] The flavonoid structure consists of a benzene condensed with a γ-pyrone ring (flavonols and flavones or its dihydro derivatives flavanols and flavanones) to which a phenyl group in position 2 is attached (see Figure 1). Green tea and, to a lesser extent, black tea, contain a number of flavonoids with significant antioxidant activity.[16,17] It is proved that drinking tea, specially green tea, is associated with a lower incidence of human cancer.[18]

The main polyphenolic components in green tea are flavanols (also known as catechins): (−)-epicatechin, *EC*; (−)-epigallocatechin, *EGC*; (−)-epicatechin gallate, *ECG;* and (−)-epigallocatechin-3-gallate, *EGCG* (Figure 2). Now it is generally accepted that the "B" ring in the flavanols, containing the catechol or the trihydroxy functionality, is responsible for most of the antioxidant activity.[16,19]

Catechins have very weak pro-oxidant effects because of their catechol functionality. Thus, it has been suggested that both hydroxyl hydrogens of the catechol can be successively abstracted, finally forming a stable quinone structure. Furthermore, it has been experimentally shown that the overall oxidative action of the green tea polyphenols involves trapping the initiating radicals ROO•, trapping the propagating lipid peroxyl radicals LOO•, and regenerating α-TocH by reducing α-Toc•.[20] This may explain the improvement/maintenance of α-TocH levels after intake of green tea, showing the antioxidant synergism of green tea polyphenols with α-TocH.[21−23]

A large body of clinical and experimental evidence have been accumulated in the last years about the antioxidative role of α-TocH and catechins by scavenging free radicals and their beneficial effects in protecting against an extensive number of diseases and aging.[15,24,25] Conversely, little theoretical work has been devoted to this subject. Very recently, dual-level kinetics calculations, using variational transition state theory including semiclassical multidimensional tunneling corrections (when needed), have been carried out to determine the mechanisms and reaction rate constants of trapping the hydroxyl and hydroperoxyl radicals by α-TocH (modeled by the 5,7,8-trimethyl-croman-6-ol molecule).[26,27] Given the nonpolar character of the natural lipid bilayer environment, those gas-phase theoretical studies were considered to be quite representative of the real problem.

From the theoretical point of view, the antioxidant activity of flavanols has been just estimated by computing the bond dissociation enthalpy (BDE) for the O−H phenolic bonds. Then it is clear that a more complete theoretical study is required to get a deeper insight in the antioxidant ability of flavanols, specially taking into account that tunneling could play an important role in the reaction. To this aim, in the present work we have used variational transition state theory including semiclassical multidimensional tunneling corrections to study the hydrogen abstraction reaction from (−)-epicatechin (*EC*) (Figure 2) by a methylperoxyl radical (CH_3OO•) as the peroxolipidic radical model.

2. Calculation Method

Geometry optimization, energies, and first and second energy derivatives of all stationary points were calculated using the hybrid metadensity functional theory.[28−32] The hybrid functional used was the MPWB1K developed by Truhlar's group.[33] This functional has been tested recently against kinetic databases, and it gives the best results for a combination of thermochemistry, thermochemical kinetics, hydrogen bonding, and weak interactions, especially for thermochemical kinetics and noncovalent interactions.[33−35] The 6-31G(d,p) basis set[36]

(15) Hollman, P. C. H.; Van Trijp, J. M. P.; Buysman, M. N. C. P.; Van der Gaag, M. S.; Mengelers, M. J. B.; Devries, J. H. M.; Katan, M. B. *FEBS Lett.* **1997**, *418*, 152−156.
(16) Pietta, P. G. *J. Nat. Prod.* **2000**, *63*, 1035−1042.
(17) Jovanovic, S. V.; Steenken, S.; Tosic, M.; Marjanovic, B.; Simic, M. G. *J. Am. Chem. Soc.* **1994**, *116*, 4846−4851.
(18) Bushman, J. L. *Nutr. Cancer* **1998**, *31*, 151−159.
(19) Silva, M. M.; Santos, M. R.; Caroco, G.; Rocha, R.; Justino, G.; Mira, L. *Free Radical Res.* **2002**, *36*, 1219−1227.
(20) Amorati, R.; Ferroni, F.; Lucarini, M.; Pedulli, G. F.; Valgimigli, L. *J. Org. Chem.* **2002**, *67*, 9295−9303.
(21) Zhou, B.; Wu, L. M.; Yang, L.; Liu, Z. L. *Free Radical Biol. Med.* **2005**, *38*, 78−84.
(22) Van Acker, F. A. A.; Schouten, O.; Haenen, G. R. M. M.; Van der Vijgh, W. J. F.; Bast, A. *FEBS Lett.* **2000**, *473*, 145−148.
(23) Jia, Z. S.; Zhou, B.; Yang, L.; Wu, L. M.; Liu, Z. L. *J. Chem. Soc., Perkin Trans. 2* **1998**, 911−915.
(24) Rietveld, A.; Wiseman, S. *J. Nutr.* **2003**, *133*, 3285−3292.
(25) Nijveldt, R. J.; Van Nood, E.; Van Hoorn, D. E. C.; Boelens, P. G.; Van Norren, K.; Van Leeuwen, P. A. M. *Am. J. Clin. Nutr.* **2001**, *74*, 418−425.
(26) Navarrete, M.; Rangel, C.; Espinosa-García, J.; Corchado, J. C. *J. Chem. Theory Comput.* **2005**, *1*, 337−344.
(27) Navarrete, M.; Rangel, C.; Corchado, J. C.; Espinosa-García, J. *J. Phys. Chem. A* **2005**, *109*, 4777−4784.
(28) Becke, A. D. *J. Chem. Phys.* **1993**, *98*, 5648−5652.
(29) Gunnarsson, O.; Lundqvist, B. I. *Phys. Rev. B* **1976**, *13*, 4274−4298.
(30) Langreth, D. C.; Perdew, J. P. *Phys. Rev. B* **1977**, *15*, 2884−2901.
(31) Kohn, W.; Becke, A. D.; Parr, R. G. *J. Phys. Chem.* **1996**, *100*, 12974−12980.
(32) Perdew, J. P. *Phys. Rev. Lett.* **1985**, *55*, 1665−11668.
(33) Zhao, Y.; Truhlar, D. G. *J. Phys. Chem. A* **2004**, *108*, 6908−6918.

was used as a unique and enough-tested set of basis functions for H-atom transfer reactions. The vibrational frequencies were obtained from the diagonalization of the corresponding MPWB1K Hessian matrices and were scaled by a factor of 0.9537.[33] The nature of all the stationary points was determined by analyzing the number of imaginary frequencies: 0 for minima and just 1 for the saddle-point.

At each stationary point we also carried out high-level single-point energy calculations at the MPWB1K/6-31G(d,p) geometries with the aim of improving the electronic description of the chemical system.

To this purpose we chose several high-level methods: (a) MPWB1K/6-311+G(2df,2p); b) projected Møller−Plesset perturbation theory[37] up to the fourth order with inclusion of single, double, and quadruple excitations: PMP4SDQ/6-31G(d,p); (c) coupled-cluster approach with single and double excitations and quasiperturbative connected triples: CCSD(T)/6-31G(d,p);[38,39] and (d) as it is well-known that the CCSD-(T) correlation method converges slowly with the increase of the basis set, we also used the CBS-QB3 approach.[40,41] In our CBS-QB3 calculations, we employed our MPWB1K geometries, instead of the B3LYP ones, as the basis for a series of single-point energy calculations and empirical corrections, to extrapolate the CCSD(T) energy to the complete basis set limit. We avoid employing the very used B3LYP functional because it has been shown that this functional may fail for H-transfer reactions.[42−46] The first high-level has been applied to both the whole system, and just to a part of it within an ONIOM scheme[47] (see Supporting Information). The PMP4SDQ, CCSD(T), and CBS-QB3 high-levels have been just used for a part of the system (20 atoms) within the same ONIOM scheme.

The MPWB1K/6-31G(d,p) H-abstraction mechanism was found to proceed via a complex in the entrance channel (which will be called reactant complex, RC), followed by a saddle-point (named SP), and a product complex, PC, in the exit channel, finally leading to the products methylhydroperoxide, CH_3OOH, and *EC* radical. To ensure connectivity between these stationary points, and to carry out the dynamical calculations, the minimum energy path (MEP)[48,49] in an isoinertial mass-weighted Cartesian coordinate system was calculated starting from the saddle-point geometry found by following the Gonzalez−Schlegel algorithm[50] at the MPWB1K/6-31G(d,p) level of theory. A step size, δs, of 0.02 bohr (where s denotes the distance along the MEP in an isoinertial mass-scaled coordinate system with a scaling mass equal to 1 amu) was used. The second derivative matrix was calculated at every two points along the MEP for $|s| < 0.2$ bohr, and at every five points for $|s| > 0.2$ bohr. Note that s is 0 at the saddle point, negative on the reactant side, and positive on the product side. The MEP of the perprotio reaction was also used for the study of the monodeuterated reaction. In both cases, the normal-mode analysis along the MEP was performed in mass-scaled Cartesian coordinates, and the reoriented dividing surface (RODS) algorithm[51] was used to improve the generalized frequencies. These generalized frequencies were also scaled using the factor mentioned above. Energy, gradient, and Hessian matrix calculations, along with geometry optimizations and MEPs were carried out using the Gaussian 03 package of programs.[52]

As it will be explained in the next section, the overall flux of the $CH_3OO\cdot + EC$ reaction is solely determined by the H-abstraction bottleneck; that is, neither the dynamical bottleneck corresponding to the $CH_3OO\cdot + EC$ association that leads to RC, nor the dynamical bottleneck corresponding to the dissociation of PC are kinetically relevant. Note, however, that the existence of a complex on the MEP that preceeds or follows the H-abstraction saddle point can be crucial in the calculation of tunneling effects. It has been shown that the explicit introduction in our calculations of those complexes[53] reduces the thickness of the classically forbidden region for energies below the adiabatic (classical potential energy + ZPE) barrier, and then tunneling is promoted and the reaction is accelerated. In this reaction the MEP on the product side reaches the adiabatic potential energy corresponding to reactants at $s = 0.39$ bohr, while the complex PC appears as far as $s = 31.7$ bohr. In these conditions, the explicit introduction in our calculations of this complex has no influence on the shape of the MEP at the region relevant for tunneling. Then just the presence of the RC can be significant for tunneling.

Direct dynamics calculations have been carried out to obtain the rate constants at different temperatures at the MPWB1K/6-31G(d,p) low-level (LL) and at the two high-levels (HL): ONIOM(CCSD(T)/6-31G(d,p):MPWB1K/6-31G(d,p)) // MPWB1K/6-31G(d,p) and ONIOM(CBS-QB3:MPWB1K/6-31G(d,p)) // MPWB1K/6-31G(d,p), which for the sake of brevity will be called from here on ONIOM−CCSD(T) and ONIOM−CBS, respectively.

At the LL the classical potential energies, geometries, and generalized frequencies were interpolated using a mapping procedure, with the exception of the five lowest generalized frequencies which have been interpolated with the IVTST0-for-frequencies scheme.[54] At the ONIOM−CCSD(T) level, the interpolated single-point energy correction (ISPE)[55,56] procedure has been used. In the ONIOM−CBS case, the HL classical potential energies on the reactant side are obtained here by adding to the LL-MEP classical potential energies a cutoff Gaussian function[54,57,58] that interpolates the energy corrections from information of the reaction path (see the Supporting Information for more details about the interpolation schemes).

All rate constants have been calculated by means of canonical variational transition state theory (CVT)[59−63] corrected with the semiclassical multidimensional small-curvature tunneling (SCT) coefficient,[64−67] using the Polyrate 9.3 code[68] (see Supporting Information for more details).

(34) Zhao, Y.; Truhlar, D. G. *J. Chem. Theory Comput.* **2005**, *1*, 415−432.
(35) Zhao, Y.; Truhlar, D. G. *J. Phys. Chem. A* **2005**, *109*, 5656−5667.
(36) Hehre, W. J.; Radom, L.; Schleyer, P. V. R.; Pople, J. A. *Ab Initio Molecular Orbital Theory;* Wiley: New York, 1986.
(37) Chen, W.; Schlegel, H. B. *J. Chem. Phys.* **1994**, *101*, 5957−5968.
(38) Raghavachari, K.; Trucks, G. W.; Pople, J. A.; Head-Gordon, M. *Chem. Phys. Lett.* **1989**, *157*, 479−483.
(39) Raghavachari, K.; Anderson, J. B. *J. Phys. Chem.* **1996**, *100*, 12960−12973.
(40) Mayer, P. M.; Parkinson, C. J.; Smith, D. M.; Radom, L. *J. Chem. Phys.* **1998**, *108*, 604−615.
(41) Montgomery, J. A. J.; Frisch, M. J.; Ochterski, J. W.; Peterson, G. A. *J. Chem. Phys.* **1999**, *110*, 2822−2827.
(42) Lynch, B. J.; Truhlar, D. G. *J. Phys. Chem. A* **2001**, *105*, 2936−2941.
(43) Zhao, Y.; Pu, J.; Lynch, B. J.; Truhlar, D. G. *Phys. Chem. Chem. Phys.* **2004**, *6*, 673−676.
(44) Malick, D. K.; Peterson, G. A.; Montomery, J. A., Jr. *J. Chem. Phys.* **1998**, *108*, 5704−5713.
(45) Kuwata, K. T.; Templeton, K. L.; Hasson, A. S. *J. Phys. Chem. A* **2003**, *108*, 11525−11532.
(46) Coote, M. L. *J. Phys. Chem. A* **2004**, *108*, 3865−3872.
(47) Maseras, F.; Morokuma, K. *J. Comput. Chem.* **1995**, *16*, 1170−1179.
(48) Truhlar, D. G.; Kupperman, A. *J. Am. Chem. Soc.* **1971**, *93*, 1840−1851.
(49) Fukui, K. *Pure Appl. Chem.* **1982**, *54*, 1825−1836.
(50) Gonzalez, C.; Schlegel, H. B. *J. Phys. Chem.* **1990**, *94*, 5523−5527.
(51) Villá, J.; Truhlar, D. G. *Theor. Chem. Acc.* **1997**, *97*, 317−323.
(52) Frisch, M. J.; et al. *Gaussian 03, revision C.02;* Gaussian, Inc.: Wallingford, CT, 2004.
(53) Masgrau, L.; González-Lafont, À.; Lluch, J. M. *J. Comput. Chem.* **1999**, *20*, 1685−1692.
(54) Hu, W. P.; Liu, Y. P.; Truhlar, D. G. *J. Chem. Soc., Faraday Trans.* **1994**, *90*, 1715−1725.
(55) Chuang, Y.-Y.; Corchado, J. C.; Truhlar, D. G. *J. Phys. Chem. A* **1999**, *103*, 1140−1149.
(56) Corchado, J. C.; no, E. L. C.; Chuang, Y. Y.; Fast, P. L.; Truhlar, D. G. *J. Phys. Chem. A* **1998**, *102*, 2424−2438.
(57) Chuang, Y. Y.; Truhlar, D. G. *J. Phys. Chem. A* **1997**, *101*, 8741−8741.
(58) Chuang, Y. Y.; Truhlar, D. G. *J. Phys. Chem. A* **1997**, *101*, 3808−3814.
(59) Garrett, B. C.; Truhlar, D. G. *J. Chem. Phys.* **1979**, *70*, 1593−1598.
(60) Garrett, B. C.; Truhlar, D. G.; Grev, R. S.; Magnuson, A. W. *J. Phys. Chem.* **1980**, *84*, 1730−1748.
(61) Isaacson, A. D.; Truhlar, D. G. *J. Chem. Phys.* **1982**, *76*, 1380−1391.
(62) Truhlar, D. G.; Isaacson, A. D.; Garrett, B. C. *Theory of Chemical Reaction Dynamics;* CRC Press: Boca Raton, FL, 1985.
(63) Fernández-Ramos, A.; Miller, J. A.; Klippenstein, S. J.; Truhlar, D. G. *Chem. Rev.* **2006**, *106*, 4518−4584.
(64) Liu, Y. P.; Lynch, G. C.; Truong, T. N.; Lu, D. H.; Truhlar, D. G.; Garrett, B. C. *J. Am. Chem. Soc.* **1993**, *115*, 2408−2415.
(65) Lu, D. H.; Truong, T. N.; Melissas, V.; Lynch, G. C.; Liu, Y. P.; Garrett, B. C.; Steckler, R.; Isaacson, A. D.; Rai, S. N.; Hancock, G. C.; Laurderdale, J. G.; Joseph, T.; Truhlar, D. G. *Comput. Phys. Commun.* **1992**, *71*, 235−262.
(66) Truhlar, D. G.; Gordon, M. S. *Science* **1990**, *249*, 491−498.

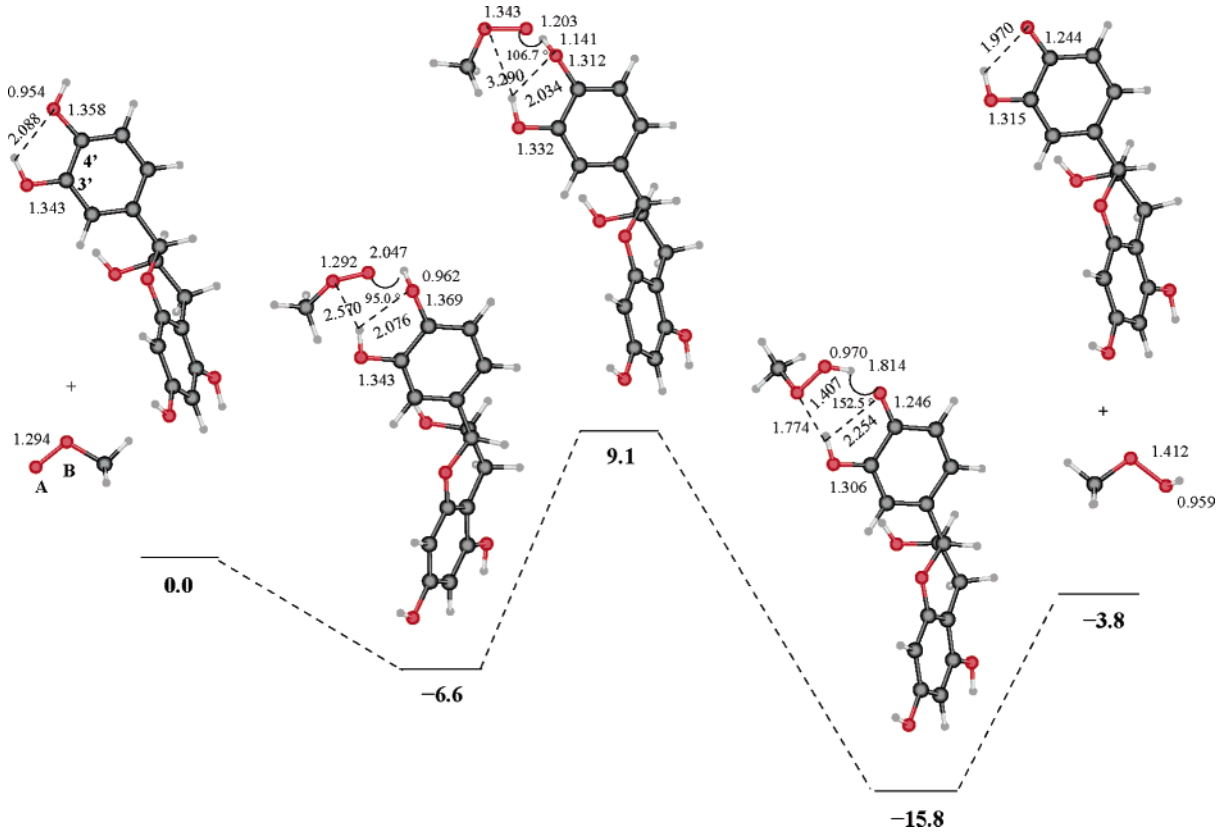

Figure 3. Optimized stationary points geometries and their classical potential-energy values, relative to reactants, in kcal/mol, calculated at the MPWB1K/6-31G(d,p) level. Oxygen atoms appear in red.

3. Results and Discussion

3.1. Stationary Points: Geometries and Relative Energies. *EC* contains five OH groups. The OH group on ring "C" is an alcoholic group to which no antioxidant ability can be ascribed. Among the four phenolic OH groups, the 3′-OH and 4′-OH groups of catechol in the "B" ring are the main groups responsible for the antioxidant activity. This results from the fact that the radical derived from the H-abstraction of any of them can be stabilized by the electron-donating power of the ortho hydroxyl and the intramolecular hydrogen bond formed. Because the ease to be abstracted has to be similar for these two OH groups, in this paper we have focused just on the abstraction of the 4′-OH group by the methylperoxyl radical, as a representative example of the antioxidant capacity of *EC*.

The optimized geometries of the stationary points located for the H-abstraction from the 4′-OH group at the MPWB1K/6-31G(d,p) level, along with the corresponding classical potential-energy profile, are shown in Figure 3. As explained in the Calculation Method section, the product complex will not be taken into account from here on in this paper.

It is worth noting that an ortho-hydroxy effect is observed: the phenolic hydrogen at position 3′ is hydrogen bonded to the oxygen at position 4′. This interaction becomes stronger as the reaction goes further, the corresponding distance going from 2.08 Å at the reactant complex to 1.97 Å at the isolated *EC* radical. Indeed, this fact is a consequence of the change of the spin distribution in the *EC* fragment, which is also increasing over the oxygen atom O_4 as the H-abstraction proceeds. The interaction between the two oxygen atoms, O_A and O_B, of the methylperoxyl fragment with the catechol functionality in *EC* is also remarkable. Two hydrogen bonds are formed between the hydrogen hydroxyls of the catechol and these oxygen atoms, leading to a very compact reactant complex and transition-state structure. At the reactant complex, the distance between the hydrogen atom of the 3′-OH group and O_B is 2.57 Å. Evolving to the transition-state structure, the $H_{3'}-O_B$ distance lengthens to 3.29 Å, at the same time opening the angle $H_{4'}-O_A-O_B$ from 95 to 107 degrees. The peroxo O_A-O_B distance becomes longer (from 1.29 to 1.41 Å) as the reaction evolves and the unpaired electron moves to the catechol moiety. At the same time the C−O bond at position 4′ is getting shorter because of the increasing electron delocalization in the catechol ring: 1.37 Å at the reactant complex, 1.31 Å at the transition-state structure, and 1.24 Å at the isolated *EC* radical, where it has an important double bond character. In turn, the C−O bond at position 3′ just shortens from 1.34 Å at the reactant complex to 1.32 Å at the final product, so indicating a weaker participation in the electron delocalization than the neighboring phenolic group at the 4′ position. The more important geometric feature is that the transition-state structure turns out to be very compact: the $O_{4'}-H_{4'}$ distance of the breaking bond is 1.14 Å, only 20% longer than in the isolated *EC*, whereas the $H_{4'}-O_A$ distance of the forming bond is 1.20 Å, only 25% longer than in the isolated methylhydroperoxide. In this way, just a short displacement, backward or forward, of the shifting hydrogen atom is required

(67) Truong, T. N.; Lu, D. H.; Lynch, G. C.; Liu, Y. P.; Melissas, V.; Stewart, J. J. P.; Steckler, R.; Garrett, B. C.; Isaacson, A. D.; González-Lafont, A.; Rai, S. N.; Hancock, G. C.; Joseph, T.; Truhlar, D. G. *Comput. Phys. Commun.* **1993**, *75*, 143−159.
(68) Corchado, J. C.; et al. *PolyRate 9.3;* University of Minnesota: Minneapolis, MN, 2004; http://comp.chem.umn.edu/polyrate.

Table 1. Low-Level and High-Level Classical (V) and Adiabatic (V_a^G) Potential Energies of the Stationary Points, Relative to Reactants, in kcal/mol

	RC		TS		products	
	V	V_a^G	$V^{\ddagger}$	$V_a^{G\ddagger}$	V	V_a^G
MPWB1K/6-31G(d,p)	−6.62	−5.27	9.05	7.01	−3.78	−3.78
MPWB1K/6-311+G(2df,2p)	−3.66	−2.31	12.60	10.56	−3.41	−3.41
ONIOM−MPWB1K[a]	−3.59	−2.24	12.56	10.52	−3.23	−3.23
ONIOM−PMP4[b]	−6.92	−5.57	23.61	21.57	1.47	1.47
ONIOM−CCSD(T)	−7.77	−6.42	12.26	10.22	−4.64	−4.64
ONIOM−CBS	−5.94	−4.59	8.04	6.00	−6.74	−6.74

[a] ONIOM (MPWB1K/6-311+G(2df,2p):MPWB1K/6-31G(d,p)) // MPWB1K/6-31G(d,p) [b] ONIOM (PMP4(SDQ)/6-31G(d,p):MPWB1K/6-31G(d,p)) // MPWB1K/6-31G(d,p)

to reach its final position with respect to the acceptor oxygen atom in *EC* (reactant) or in methylhydroperoxide (product), respectively. In contrast, the reported[26] H-abstraction transition-state structure for the α-TocH + HOO· reaction, at the BH&HLYP/6-31G electronic structure level, was clearly reactant-like and much less compact, that is, the bond being broken was about 11% larger than in the reactants while the bond being formed was 41% larger than in the products.

In Table 1 the energetics for the three regions (reactants association, H-transfer, and dissociation to final products) taken into account in our study of the *EC* + CH_3OO· reaction, are given at the different levels of theory used in our calculations. As already indicated, the abstraction of the phenolic hydrogen at the 4′ position takes place via the formation of a complex in the entrance channel (RC, depicted in Figure 3). Its relatively high stabilization is mainly due to the two hydrogen-bonded interactions, described before, between the two oxygen atoms, O_A and O_B, of the methylperoxyl fragment and the catechol functionality in *EC*. The LL-RC stabilization decreases by 3 kcal/mol when the basis set is extended, perhaps indicating a basis set superposition error at the LL (MPW1BK/6-31G (d,p)). The LL-H-abstraction classical potential-energy barrier is rather high (9.05 kcal/mol) and it rises up to 12.6 kcal/mol when the basis set is extended. This high-energy barrier causes the global flux of the *EC* + CH_3OO· reaction to be, in practice, solely determined by the H-abstraction bottleneck, as already explained in the previous section. The increase in H-abstraction barrier heights in going from a double-ξ to a triple-ξ basis set had already been reported for the α-TocH + HOO· reaction at the BH and HLYP level.[26] However, in that same study it was also verified that further changes within triple-ξ basis sets did only modify the computed magnitudes by about 1 kcal/mol. As for the reaction energy for the H-abstraction process, the two MPW1BK calculations give nearly the same value (around −3.5 kcal/mol in adiabatic potential energy). Unfortunately, there is no experimental reported value for the reaction energy of the H-abstraction reaction between *EC* and CH_3OO·, although an estimated value can be obtained from the difference between bond dissociation energies: ΔBDE(O−H).

Taking into account the value of 86.9 ± 1.0 kcal/mol reported for the O−H BDE of CH_3OOH[69] and two of the most recent results for catechol, both experimental[70](82.5 ± 1.2 kcal/mol) and theoretical[71] (81.5 kcal/mol at a basis-set extrapolated CCSD level), the estimated values for the *EC* + CH_3OO· reaction would be −4.4 ± 2.2 kcal/mol[70] and −5.4 ± 1.0 kcal/mol,[71] respectively (see Supporting Information for more details).

The second high-level calculation shown in Table 1 corresponds to an ONIOM scheme where the low-level electronic energy for the model and the real system were calculated at the MPW1BK/6-31G(d,p) level, and the high-level electronic energy for the model system was obtained at the MPWB1K/6-311+G(2df,2p) level. The comparison between the figures in the second and third rows of Table 1 indicates that the selected ONIOM partition is very adequate to properly describe the energetic properties of the *EC* + CH_3OO· reaction. However, as the MPWB1K functional was neither developed nor calibrated for any of these flavonoid systems, higher-level ab initio single-point energy calculations within the ONIOM scheme were imperative before carrying out any dynamical study of the reaction process. At this point, it must be remarked that the *EC* + CH_3OO· system presents severe spin contamination problems along the reaction path. In particular, the expected value of $\hat{S}^2$ for the UHF wave function ranges from 0.75 at RC to 1.25 at the saddle point. To solve the spin contamination problem, the third high-level method tried out to correct the DFT energies was the PMP4 formulism. Although the spin projected fourth-order Møller−Plesset perturbation theory properly eliminates the contamination of higher-spin states, the PMP4 H-abstraction barrier obtained is clearly too high and the reaction energy is not well described either. For this reason the PMP4 method was not adopted for the rate constant calculations of the *EC* + CH_3OO· reaction carried out in this paper. The fourth high-level method used in this study has been the CCSD(T) approach which is expected to be more reliable than the PMP4 method. In addition, the CCSD method is rather orbital insensitive, and one may expect that performing CCSD calculations with an unrestricted reference would reduce spin contamination considerably. As indicated by Stanton,[72] spin contamination in the CCSD method for doublet radicals is indeed very small in both ROHF and UHF CCSD calculations, even when the UHF spin-contamination is very large. The values in Table 1 for the ONIOM−CCSD(T) method, reflect a bigger stabilization of RC and a slightly more negative reaction energy than the DFT values, in agreement with the most recent experimental[70] and theoretical[71] estimations commented above. In contrast, the H-abstraction barrier height turns out to be nearly the same than the MPWB1K/6-311+G(2df,2p) one. The 4′-OH *EC* BDE, calculated here using an isodesmic approach[73] turns out to be 77.6 and 78.9 kcal/mol at the MPWB1K/6-311+G(2df,2p) and the ONIOM−CCSD(T) levels, respectively. These calculated values may be somewhat underestimated owing to the error of the DFT method and the basis set used at the CCSD(T) level. It is well-known that the CCSD(T) approach converges smoothly but very slowly as the basis set used is increased. However, CCSD(T) calculations with a more extended basis set on the model system (11 heavy atoms and 9 hydrogens) would be rather costly. Practical considerations preclude such a brute-force attack on the problem, and composite methods become then a very useful alternative. The last high-level method tested has been

(69) Blanksby, S. J.; Ramond, T. M.; Davico, G. E.; Nimlos, M. R.; Kato, S.; Bierbaum, V. M.; Lineberger, W. C.; Ellison, G. B.; Okumura, M. *J. Am. Chem. Soc.* **2001**, *123*, 9585−9596.
(70) Correia, C. F.; Guedes, R. C.; Dossantos, R. M. B.; Cabral, B. J. C.; Simoes, J. A. M. *Phys. Chem. Chem. Phys.* **2004**, *6*, 2109−2118.
(71) Cabral, B. J. C.; Canuto, S. *Chem. Phys. Lett.* **2005**, *406*, 300−305.
(72) Stanton, J. F. *J. Chem. Phys.* **1994**, *101*, 371−374.
(73) Lucarini, M.; Pedulli, G. F.; Guerra, M. *Chem.—Eur. J.* **2004**, *10*, 933−939.

Table 2. Rate Constants (in M^{-1} s^{-1}) and SCT Transmission Coefficients Computed at the MPWB1K/6-31G(d,p) (Low-Level) Electronic-Structure Level of Theory as a Function of Temperature

T (K)	k^{TST}	k^{CVT}	κ^{SCT}	$k^{CVT/SCT}$
150	2.21×10^{-5}	2.20×10^{-5}	2.87×10^{8}	6.26×10^{3}
200	1.02×10^{-2}	1.02×10^{-2}	8.59×10^{5}	8.61×10^{3}
300	5.85	5.76	2.89×10^{3}	1.62×10^{4}
400	1.68×10^{2}	1.63×10^{2}	1.91×10^{2}	2.98×10^{4}
500	1.43×10^{3}	1.37×10^{3}	4.15×10^{1}	5.43×10^{4}
600	6.56×10^{3}	6.26×10^{3}	1.60×10^{1}	9.57×10^{4}

Table 3. Rate Constants (in M^{-1} s^{-1}) and SCT Transmission Coefficients Computed at the ONIOM−CCSD(T) (High-Level) Electronic-structure Level of Theory as a Function of Temperature.

T (K)	k^{TST}	k^{CVT}	κ^{SCT}	$k^{CVT/SCT}$
150	2.96×10^{-10}	2.87×10^{-10}	1.10×10^{13}	3.13×10^{3}
200	2.36×10^{-6}	2.29×10^{-6}	1.91×10^{9}	4.35×10^{3}
300	2.32×10^{-2}	2.26×10^{-2}	3.72×10^{5}	8.25×10^{3}
400	2.76	2.67	5.88×10^{3}	1.53×10^{4}
500	5.52×10^{1}	5.31×10^{1}	5.40×10^{2}	2.78×10^{4}
600	4.47×10^{2}	4.28×10^{2}	1.19×10^{2}	4.90×10^{4}

Table 4. Rate Constants (in M^{-1} s^{-1}) and SCT Transmission Coefficients Computed at the ONIOM−CBS (High-Level) Electronic-structure Level of Theory as a Function of Temperature.

T (K)	k^{TST}	k^{CVT}	κ^{SCT}	$k^{CVT/SCT}$
150	7.40×10^{-4}	7.30×10^{-4}	1.66×10^{7}	1.21×10^{4}
200	1.43×10^{-1}	1.42×10^{-1}	1.20×10^{5}	1.67×10^{4}
300	3.39×10^{1}	3.34×10^{1}	9.74×10^{2}	3.15×10^{4}
400	6.26×10^{2}	6.08×10^{2}	9.86×10^{1}	5.71×10^{4}
500	4.09×10^{3}	3.94×10^{3}	2.70×10^{1}	1.01×10^{5}
600	1.58×10^{4}	1.51×10^{4}	1.20×10^{1}	1.72×10^{5}

then the CBS-QB3 composite method of Petersson and coworkers[40,41] that uses a series of single-point energy calculations to extrapolate the CCSD(T) energy to the complete basis-set limit. Recent studies indicate that CBS-QB3 often provides excellent agreement with experimental reaction energies and barriers, in some cases with greater accuracy than single-point energy CCSD(T) calculations with polarized triple-ξ basis sets.[74−78] On the other hand, it has been reported that CBS-QB3 systematically underestimates intermolecular hydrogen-transfer barriers in monoradicals by ~0.5 kcal/mol, as compared to the very high level W1 method of Martin et al.,[79] perhaps because CBS-QB3 overcompensates for the effects of spin contamination in open-shell systems.[46] The figures in Table 1 show that the ONIOM−CBS method gives the lowest H-abstraction classical energy barrier and the most negative reaction energy for the *EC* + $CH_3OO\cdot$ reaction, this last result being close to the lowest experimental[70] and theoretical[71] values given earlier. In any case, flavonoid reactivity has never been systematically analyzed by high-level ab initio structure calculations, and for this reason we decided to carry out dynamical calculations on both the ONIOM−CCSD(T) and the ONIOM−CBS potential-energy surfaces in spite of the 4 kcal/mol difference in the corresponding H-abstraction barrier heights.

3.2. Reaction Path and Rate Constant Analysis. In Tables 2, 3, and 4, respectively, the LL, ONIOM−CCSD(T), and the ONIOM−CBS one-way flux rate constants for the H-abstraction are presented along with the tunneling transmission coefficients as a function of temperature. The conventional transition-state rate constants values, k^{TST} (T), at the three levels of theory, are mainly due (besides entropic contributions) to the high classical potential-energy barriers given in Table 1. At 150 K, the ONIOM−CCSD(T) rate constant is 5 orders of magnitude smaller than the LL and ONIOM−CBS ones, but this difference reduces to 1−2 orders of magnitude when temperature is increased up to 600 K and entropic effects become more significant. (Note that the ONIOM−CCSD(T) k^{TST} (T) are, in fact, calculated at the classical potential-energy maximum on the high-level MEP following the ISPE method. However, in this case the ISPE results, $s(V_{max}) = 0.025$ bohr; $V_{max} = 12.5$ kcal/mol, do not differ much from the ones calculated at the LL H-abstraction saddle point).

Variational effects are small at the three levels of theory. For instance, they slow the ONIOM−CBS rate constants by only a factor of 0.99 and 0.96 at 150 and 600 K, respectively.

The most striking result of our dynamical calculations corresponds to the huge values obtained for the SCT transmission coefficients. The transmission coefficient values at the ONIOM−CCSD(T) level are the biggest among the three levels of calculation and range from 1.19×10^2 at 600 K, up to 1.10×10^{13} at 150 K, whereas the lowest values, although still very big, are obtained with the ONIOM−CBS methodology: 1.20×10^1 at 600 K, and 1.66×10^7 at 150 K.

The reason for those enormous SCT transmission coefficients must be found on the shape of the adiabatic potential-energy profiles along the reaction path (Figure 4). It can be observed that the adiabatic potential-energy barriers are extremely narrow at the three levels of theory but specially at the ONIOM−CCSD-(T) level, which presents the highest adiabatic barrier (V^{AG} = 10.43 kcal/mol; $s(V^{AG}) = 0.025$ bohr) (see refs 80 and 81 for recent examples of other systems with large tunneling contributions due to narrow potential-energy barriers). The LL and ONIOM−CBS widths of the adiabatic potential-energy profiles are more alike because the ONIOM−CBS MEP was obtained by interpolation using the HL information calculated only at the stationary points. Nevertheless, the adiabatic barrier is slightly higher at the LL level ($V^{AG} = 7.04$ kcal/mol; $s(V^{AG}) = 0.0025$ bohr) than at the ONIOM−CBS level ($V^{AG} = 6.00$ kcal/mol; $s(V^{AG}) = 0.0021$ bohr). The shape of those adiabatic energy profiles clearly reflects the very short path length of the shifting hydrogen between its initial position at the RC complex and its final position at the methylhydroperoxide structure, a short distance that has already been remarked here from the comparison of the corresponding stationary-point geometries. On the ONIOM−CCSD(T) profile the adiabatic potential energy drops around 10 kcal/mol from the transition-state structure at $s = 0$ bohr to $s = -1.0$ bohr and to $s = 0.5$ bohr in the backward and forward directions, respectively. At those geometries on the MEP, the H-transfer can be considered to be completed, and further away the system undertakes a long path characterized by the heavy atom reorganization and a slow decrease of the adiabatic potential energy to finally attain the geometry and

(74) Gomez-Balderas, R.; Coote, M. L.; Henry, D. J.; Radom, L. *J. Phys. Chem. A* **2004**, *108*, 2874−2883.
(75) Henry, D. J.; Parkinson, C. J.; Radom, L. *J. Phys. Chem. A* **2002**, *106*, 7927−7936.
(76) Guner, V.; Khuong, K. S.; Leach, A. G.; Lee, P. S.; Bartberger,M. D.; Houk, K. N. *J. Phys. Chem. A* **2003**, *107*, 11445−11459.
(77) Kuwata, K. T.; Hasson, A. S.; Dickinson, R. V.; Petersen, E. B.; Valin, L. C. *J. Phys. Chem. A* **2005**, *109*, 2514−2524.
(78) Hasson, A. S.; Chung, M. Y.; Kuwata, K. T.; Converse, A. D.; Krohn, D.; Paulson, S. E. *J. Phys. Chem. A* **2003**, *107*, 6176−6182.
(79) Martin, J. M. L.; Oliveira, G. D. *J. Chem. Phys.* **1999**, *111*, 1843−1856.

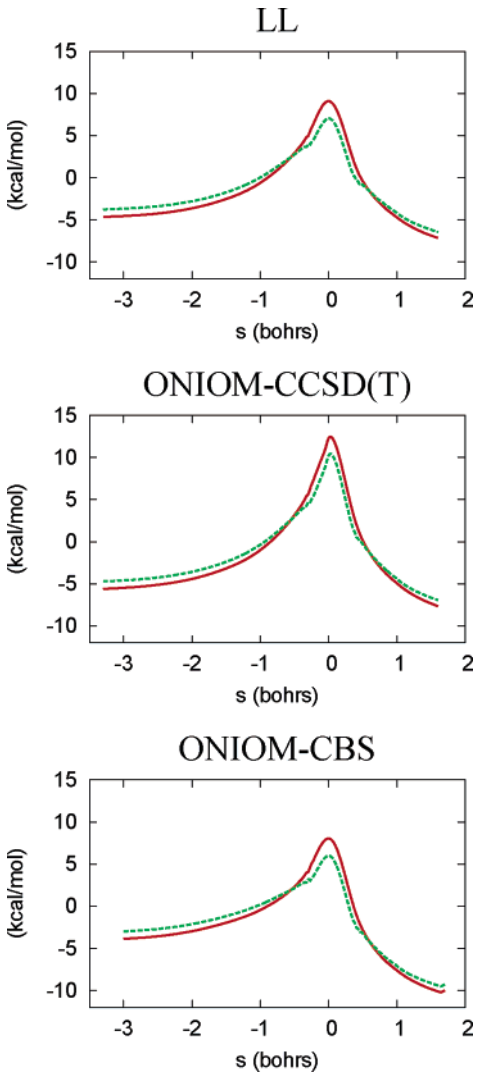

Figure 4. Classical potential-energy profile (MEP, red solid line) and adiabatic energy profile (V_a^G, green dashed line) at three different levels of calculation. Energies are relative to reactants.

energy values corresponding to RC and the final products. This compact doubly hydrogen-bonded complex between *EC* and $CH_3OO\cdot$ that forces such a short H-transfer path length, is not present in other radical scavenging reactions because the antioxidant molecule does not contain a catechol functionality (for instance, ubiquinol/α-TocH plus HOO· reactions[26,82]). To shed light in this point, we have compared the MEPs corresponding to the *EC* + $CH_3OO\cdot$ and α-TocH + $CH_3OO\cdot$ reactions, calculated at the MPWB1K/6-31G(d,p) low-level (LL). We have modeled the α-tocopherol molecule by the 2,2,5,7,8-pentamethylcroman-6-ol molecule (that is, we have replaced the trimethyltridecyl chain attached to carbon 2 in the α-tocopherol molecule by a methyl group). Figure 5 clearly shows that the MEP corresponding to the α-TocH case is wider. Confirming this fact, the unscaled imaginary frequencies at the saddle point are 1827i and 2501i cm^{-1} for α-TocH and *EC* reactions, respectively. Because the α-TocH MEP turns out to be lower and wider than the *EC* MEP, the SCT transmission

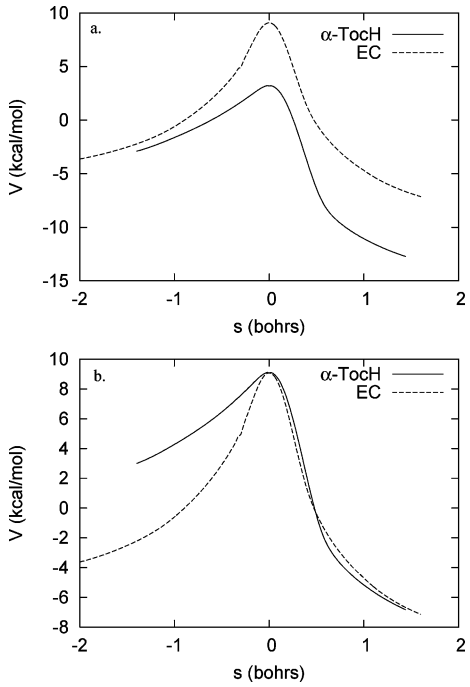

Figure 5. α-tocopherol and *EC* MEPs. (a) Energies are relative to the corresponding reactants. (b) The α-tocopherol MEP has been moved up to make easier the comparison of the respective widths.

coefficient for the α-TocH + $CH_3OO\cdot$ reaction is expected to be notoriously smaller than for the *EC* + $CH_3OO\cdot$ reaction.

In fact, without tunneling corrections, the variational H-abstraction rate constants at 300 K, k^{CVT} (T = 300 K), at the LL (5.76 M^{-1} s^{-1}) and the ONIOM−CCSD(T) (2.26 × 10^{-2} M^{-1} s^{-1}) level of theory would be smaller than the H-transfer reaction rate constant of reaction 3 (typically 10^1 M^{-1} s^{-1}) and the ONIOM−CBS k^{CVT} (T) would be only somewhat greater (33.4 M^{-1} s^{-1}). In any case, our results show that tunneling effects are responsible for making the *EC* + $CH_3OO\cdot$ reaction (as a model for the *EC* + LOO· process) clearly much faster than reaction 3, so then *EC* would become able to break the free-radical chain-lipid peroxidation reaction by trapping the LOO· radical. At this point it has to be remarked that this decisive role of tunneling cannot be recognized when just BDE data are handled.

It should be remarked that the actual *EC* + $CH_3OO\cdot$ reaction does not take place in gas phase. The scavenging of the lipid peroxyl radicals LOO· by *EC* or α-TocH occurs in the lipid bilayers of cell membranes, where the dielectric constant is much less than for bulk water. So, dielectric constants around 30 for the lipid head group-water interface and around 10 for the ester group region have been suggested.[83] Because of that and taking into account that *EC* + $CH_3OO\cdot$ is not an ionic but a free-radical reaction, the environmental effects should not alter significantly the main conclusions of the present paper which have been obtained by gas-phase calculations. To test this hypothesis we have incorporated the environmental effects by means of the separable equilibrium solvation (SES) approximation.[84] In the SES approximation one first calculates the MEP in the gas phase and then solvates the system at geometries

(80) Tautermann, C. S.; Loferer, M. J.; Voegele, A. F.; Liedl, K. R. *J. Phys. Chem. B* **2003**, *107*, 12013−12020.
(81) Tejero, I.; Garcia-Viloca, M.; González-Lafont, À.; Lluch, J. M.; York, D. M. *J. Phys. Chem. B* **2006**, *110*, 24708−24719.
(82) Espinosa-García, J. *J. Am. Chem. Soc.* **2004**, *126*, 920−927.
(83) Zhou, F.; Schulten, K. *J. Phys. Chem.* **1995**, *99*, 2194−2207.
(84) Chuang, Y.-Y.; Cramer, C. J.; Truhlar, D. *Int. J. Quantum Chem.* **1998**, *70*, 887−896.

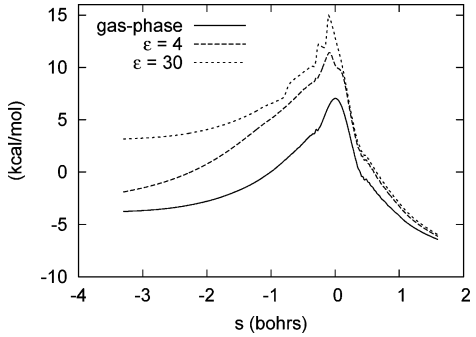

Figure 6. Effective potentials for tunneling corresponding to the gas-phase reaction, and including environmental effects with $\epsilon = 4$ and $\epsilon = 30$. Energies are relative to the corresponding reactants.

Table 5. SCT Transmission Coefficients for the Gas-Phase Reaction, Including Environmental Effects with $\epsilon = 4$ and $\epsilon = 30$, at Different Temperatures

T (K)	gas-phase	$\epsilon = 4$	$\epsilon = 30$
150.00	2.87×10^{8}	5.81×10^{11}	2.35×10^{13}
200.00	8.59×10^{5}	7.93×10^{7}	1.89×10^{9}
263.00	1.40×10^{4}	1.99×10^{5}	3.44×10^{6}
298.15	3.10×10^{3}	2.42×10^{4}	3.54×10^{5}
300.00	2.89×10^{3}	2.20×10^{4}	3.19×10^{5}
400.00	1.91×10^{2}	5.87×10^{2}	5.51×10^{3}
500.00	4.15×10^{1}	8.39×10^{1}	5.56×10^{2}
600.00	1.60×10^{1}	2.61×10^{1}	1.31×10^{2}

along the gas-phase MEP by adding the standard-state molar free energy of solvation to the gas-phase potential energy.

In the present case the standard-state molar free energy of solvation has been calculated using the conductor-like formalism of the polarized continuum model (CPCM) developed by Barone et al.,[85] at the MPWB1K/MG3S level. For these CPCM calculations, a value of 4 and 30 was employed for the dielectric constant, to simulate the hydrophobic interior of a lipid membrane and the outer part of the interface lipid/water, respectively.[83] The ISPE method[55] has been used to interpolate the solvation correction along the MEP.

We have employed the zero-order canonical mean shape (CMS-0) approximation[86] to calculate the tunneling effects. So, the SCT calculations have been carried out with an effective potential for tunneling which is obtained by adding the gas-phase adiabatic potential energy and the standard-state free energy of solvation[87] (Figure 6). When comparing the three curves shown in Figure 6, we must note that the profiles with $\epsilon = 4$ and $\epsilon = 30$ also include solvent-free energy contributions, whereas the gas-phase curve is just an adiabatic potential-energy profile.

The SCT transmission coefficients for gas-phase, and including environmental effects ($\epsilon = 4$ and $\epsilon = 30$), at different temperatures are given in Table 5. Because of the environment, the effective potentials for tunneling become higher, this way leading to bigger SCT transmission coefficients than in gas phase. So, our estimation of the environmental effects confirms the key role of tunneling effects in this *EC* + $CH_3OO\cdot$ reaction.

In Table 6 the primary kinetic isotope effects (KIEs) for the H-abstraction reaction between *EC* and $CH_3OO\cdot$ are given as a function of temperature at the three levels of calculation used in this dynamical treatment. This KIE arises from the substitution of the hydrogen at the 4′ position by a deuterium. The three methodologies give large normal KIEs that decrease as temperature increases, the ONIOM−CCSD(T) KIEs being the largest ones at each temperature. The relative weight of the different factors that contribute to the total KIE was analyzed by the factorization given in eq 6:

Table 6. Kinetic Isotope Effects (KIEs) as a Function of Temperature, at the Three Different Levels of Theory.

T (K)	MPWB1K/6-31G(d,p)	ONIOM:CCSD(T)	ONIOM:CBS
150	12.92	26.64	11.30
200	12.07	12.63	10.24
300	10.17	11.41	8.18
400	8.04	9.68	6.64
500	6.42	7.94	5.38
600	5.19	6.49	4.46

$$\mathrm{KIE}(T) = \frac{k_{\mathrm{H}}^{\mathrm{CVT/SCT}}(T)}{k_{\mathrm{D}}^{\mathrm{CVT/SCT}}(T)} = \frac{\kappa_{\mathrm{H}}^{\mathrm{SCT}}(T)}{\kappa_{\mathrm{D}}^{\mathrm{SCT}}(T)} \frac{k_{\mathrm{H}}^{\mathrm{CVT}}(T)}{k_{\mathrm{D}}^{\mathrm{CVT}}(T)} = \mathrm{KIE}_{\mathrm{tun}}\mathrm{KIE}_{\mathrm{CVT}} \quad (6)$$

where $\mathrm{KIE}_{\mathrm{tun}}$ corresponds to the ratio of SCT transmission coefficients of the perprotio and the deuterated *EC* + $CH_3OO\cdot$ reactions. While $\mathrm{KIE}_{\mathrm{tun}}$ accounts for the tunneling contribution to the global KIE, $\mathrm{KIE}_{\mathrm{CVT}}$ is the ratio of the CVT rate constants for the perprotio and the deuterated reactions evaluated at the corresponding generalized transition states and accounts for the translational, vibrational, rotational, electronic, and the Boltzmann factor (associated with the classical potential energy) contributions to the global KIE. At the ONIOM−CBS level, the global KIE at 300 K is 8.18, and its factorization gives $\mathrm{KIE}_{\mathrm{tun}} = 1.11$ and $\mathrm{KIE}_{\mathrm{CVT}} = 7.37$. So the differences between the two generalized transition-state partition functions and the two reactant partition functions (being those differences mainly due to the vibrational degrees of freedom) account by themselves for as much as the 90% of the global KIE. That small contribution of tunneling to the KIE might seem to be in disagreement with the huge SCT transmission coefficients reported above. The point here is that both the perprotio and the deuterated *EC* + $CH_3OO\cdot$ reactions present very large tunneling effects in this reaction, but because of the narrowness of the adiabatic potential-energy profile, those SCT transmission coefficients are very similar for both hydrogen and deuterium and nearly cancel out in the calculation of their KIE contribution (see ref 81 for a discussion of this point in the H-abstraction catalyzed by soybean lipoxygenase-1, a reaction which also has very large tunneling contributions.)

Finally, we have calculated the representative tunneling energies (RTEs) for both the perprotio and the deuterated reactions at the ONIOM−CBS level. At a given temperature, the RTE is the energy which mostly contributes to the SCT transmission coefficient. It is a consequence of the opposite trends of the quantal transmission probability and the Boltzmann factor as a function of the energy. At 300 K, it turns out to be only 0.01 and 0.69 kcal/mol above the adiabatic energy of reactants for the H and D transfers, respectively (0.07 and 2.80 kcal/mol at 600 K, respectively). These so small RTE values indicate that tunneling is already very easy at the adiabatic energies of reactants, a consequence of the narrowness of the adiabatic potential-energy profile.

(85) Barone, V.; Cossi, M. *J. Phys. Chem. A* **1998**, *102*, 1995−2001.
(86) Truhlar, D. G.; Liu, Y.-P.; Schenter, G. K.; Garrett, B. C. *J. Phys. Chem.* **1994**, *98*, 8396−8405.
(87) Chuang, Y.-Y.; Radhakrishnan, M. L.; Fast, P. L.; Cramer, C. J.; Truhlar, D. G. *J. Phys. Chem. A* **1999**, *103*, 4893−4909.

4. Conclusions

It is well-known that the polyphenolic compounds abundantly contained in green tea, specially catechins, exert protective effects against cancer, inflammatory and cardiovascular diseases, and aging. These protective effects have been mainly attributed to their antioxidant activity by scavenging free radicals: catechins effectively suppress the lipid peroxidation in biological issues and subcellular fractions. It seems that the catechol moiety of catechins with its dihydroxy functionality is most responsible for that antioxidant capacity.

In this paper we have combined high-level electronic structure calculations and canonical variational transition state theory including semiclassical multidimensional small-curvature tunneling corrections to study the mechanism and to calculate the reaction rate constants of the hydrogen abstraction reaction from (−)-epicatechin by methylperoxyl radical, taken as a peroxolipidic radical model.

Our results have allowed us to understand one of the key factors of the antioxidant effectiveness of the catechol group. Because of the existence of the two hydroxyl groups in an ortho disposition at the "B" ring, two hydrogen bonds are formed between the hydrogen hydroxyls and the two oxygen atoms of the attacking methylperoxyl radical, therefore leading to very compact structures corresponding to a reactant complex prior to the H-abstraction process and the transition-state structure of the reaction. This way the H-abstraction occurs as though it was an intramolecular H-transfer within the reactant complex, involving an extremely short path length. The resulting adiabatic potential-energy profile turns out to be extraordinarily narrow in the range of energies that makes tunneling possible (that is, at the energy corresponding to reactants and above it). As a consequence, the H-abstraction process from catechin takes place with a huge tunneling effect. This reaction becomes then fast enough to trap the lipid peroxyl radicals in a dominant competition with the very damaging free-radical chain-lipid peroxidation reaction. Quantum-mechanical tunneling is then the clue of the high antioxidant activity of molecules containing the catechol group, so explaining the important benefits of drinking green tea known in eastern Asia for thousands of years.

Acknowledgment. We are grateful for financial support from the Spanish "Ministerio de Educación y Ciencia" and the "Fondo Europeo de Desarrollo Regional" through project CTQ2005-07115/BQU and the Generalitat de Catalunya (Grant 2005SGR00400). We also thank CESCA for the computational facilities.

Supporting Information Available: Complete refs 52 and 68; details for the ONIOM calculations, together with Figure S1, which shows the spin distribution diagram; computational details for the different interpolation schemes used; the specific formulation of the CVT/SCT rate constant; results corresponding to the O−H bond dissociation energies. This material is available free of charge via the Internet at http://pubs.acs.org.

JA063766T